Surface Topography: Metrology and Properties

ACCEPTED MANUSCRIPT

Effect of FSP on mechanical properties, wear and Corrosion behavior of A356 Al Alloy

To cite this article before publication: Khadija M. Hasona *et al* 2021 *Surf. Topogr.: Metrol. Prop.* in press https://doi.org/10.1088/2051-672X/abf328

Manuscript version: Accepted Manuscript

Accepted Manuscript is "the version of the article accepted for publication including all changes made as a result of the peer review process, and which may also include the addition to the article by IOP Publishing of a header, an article ID, a cover sheet and/or an 'Accepted Manuscript' watermark, but excluding any other editing, typesetting or other changes made by IOP Publishing and/or its licensors"

This Accepted Manuscript is **© 2021 IOP Publishing Ltd**.

During the embargo period (the 12 month period from the publication of the Version of Record of this article), the Accepted Manuscript is fully protected by copyright and cannot be reused or reposted elsewhere.
As the Version of Record of this article is going to be / has been published on a subscription basis, this Accepted Manuscript is available for reuse under a CC BY-NC-ND 3.0 licence after the 12 month embargo period.

After the embargo period, everyone is permitted to use copy and redistribute this article for non-commercial purposes only, provided that they adhere to all the terms of the licence https://creativecommons.org/licences/by-nc-nd/3.0

Although reasonable endeavours have been taken to obtain all necessary permissions from third parties to include their copyrighted content within this article, their full citation and copyright line may not be present in this Accepted Manuscript version. Before using any content from this article, please refer to the Version of Record on IOPscience once published for full citation and copyright details, as permissions will likely be required. All third party content is fully copyright protected, unless specifically stated otherwise in the figure caption in the Version of Record.

View the article online for updates and enhancements.

This content was downloaded from IP address 185.13.112.71 on 06/04/2021 at 13:17

Effect of FSP on mechanical properties, wear and Corrosion behavior of A356 Al Alloy

Khadija M. Hasona[1], Rasha M. Afify[1], El-Sayed H. Mansour[1], Ahmed M. Gaafer[1], Tamer S. Mahmoud[1], and Ahmed O. Mosleh[1,2*]

[1]*Mechanical Engineering Department, Faculty of Engineering at Shoubra, Benha University, Cairo, Egypt.*

[2]*National University of Science and Technology "MISiS", Leninsky Prospekt, 4, Moscow 119049, Russian Federation*

[*] corresponding author

Abstract

Grain refining and microstructure homogenization are fundamental challenges for enhancing the performance of the materials. One of the effective ways to solve these challenges is the Friction stir processing (FSP) technique. This paper investigates the FSP parameters' impact on the microstructure, hardness, wear, and corrosion behavior of A356 Al-Si cast alloy. The FSP parameters are rotational speed (355-900 rpm), trasverse speed (10-40 mm/min), and two different tool geometries. The results revealed that the intense plastic deformation and dynamic recrystallization fragmented the needle-shaped eutectic silicon particles. The particle size change was more pronounced as the rotational speed was increased than the transverse speed and the pin profile tool geometry. The fragmented and homogeneously distributed Si particles in the investigated alloy increased their hardness, wear, and corrosion resistance compared with those of the unprocessed base metal. The hardness increased by two times, and the wear rate reduced by ten times, while the corrosion rate decreased by 200 times than the BM at lower tool rotational speeds and higher transverse speed. The Possible reasons were discussed for these enhancements.

Keywords

Friction stir welding (FSP); Microstructure characterization; hardness; wear resistance; corrosion resistance.

Accepted Manuscript

Nomenclature

FSP	Friction stir processing	CNC	Computer numerical control
TCP	Threaded cylindrical pin	SCCP	Square pin with a cylindrical corners pin
SZ	Nugget or stirred zone	Rp	Resistance polarization
BM	Base metal	TMAZ	Thermomechanical affected zone
HAZ	Heat-affected zone	OM	Optical microscopy
SEM	Scanning electron microscopy	RS	Retreating side
AS	Advancing side	E_{corr}	Corrosion potential
EDX	Energy-dispersive X-ray	Al_2O_3	Aluminum oxide
SiO_2	Silicon oxide	DRX	Dynamic recrystallization
YS	Yield strength	UTS	Ultimate tensile strength
EL.	Elongation	WR	Wear rate
COE	Coefficient of friction		

1. Introduction

Al-Si alloys exhibit high thermal conductivity, low thermal coefficient of expansion, high strength, lightweight, and good wear resistance. They are extensively used in the automotive and aerospace industries [1–8]. Engine parts, pistons, connecting rods, marine fittings, housings, and water manifolds are examples of parts made of these alloys [9,10]. Al-Si-based alloys' main disadvantages, when used for casting methods, are pores: entertained oxide film, massive primary silicon particle segregation, coarse eutectic structure, and unfavorable shrinkage behavior [11–13]. Such defects can be reduced by transforming the coarse primary silicone into fine particles and removing porosities by FSP [14].

FSP is a thermomechanical processing technique, which changes the material's microstructural and mechanical properties [15,16]. The process parameters, such as transverse speed, rotational speed, and tool geometry, need to be controlled to achieve the desired fine grain size. Many studies underway research the impact of these process parameters on the grain structure [10,17–20]. Ma et al. [21] investigated the effects of FSP on the microstructural characteristics of the A356 cast aluminum alloy. FSP refines the cast

Accepted Manuscript

microstructure, eliminates the porosity, and produces a microstructure with fine Si particles (0.25 – 0.42μm distributed in a fine grain aluminum matrix (3 - 4μm) [21]. Karthikeyan et al. [22] studied the impact of single FSP process variables on the mechanical properties and microstructural features of cast aluminum alloy A319. The authors found that the FSP increases the yield strength by 13%, enhances the tensile strength by 20% to 50%, and increases the ductility from 1.5 to 5 times compared with as-cast A319 alloy. Saini et al. [23] investigated the impact of different transverse speeds on the cast Al-17%Si Alloys' surface characteristics at fixed rotational tool speed. Eutectic and primary Si particles were refined and normally distributed. Furthermore, the tensile and hardness properties were enhanced, and the EL was increased from < 2% to about 9%. Santella et al. [24] investigated the impact of FSP on the mechanical properties of A356 and A319 Al cast alloys. The cast dendritic structure had been replaced by a fine equiaxed structure in the stirred zone. The tensile strength, ductility, and fatigue life were enhanced by the FSP [24].

Fewer studies were focused on the influence of FSP on the wear behavior of Al–Si cast alloys [14,22,25–27]. Aktarer et al. [25] reported that the FSP of Al-12%Si cast alloy exhibited higher mechanical properties and wear resistance than the base alloy. Reddy et al. [26] investigated the effect of FSP on the tribological characteristics of as-cast A356 alloy. The A356 FSP displayed excellent resistance to wear. Alidokht et al. [28] investigated the effect of FSP on wear resistance of cast A356 aluminum alloy at various rotation rates. The results revealed that the wear resistance of as-cast A356 alloy significantly improved by performing FSP. Furthermore, the samples with high rotation rates display slightly higher wear resistance than the samples processed at lower rotation rates. This can be related to higher hardness due to a uniformed and refined microstructure, i.e., a significant modification in the size, distribution, and morphology of Si particles.

Little studies have been carried out on the influence of FSP on the corrosion behavior of Al-Si cast alloys [24,29–33]. Essential and valuable information is provided by using Potentiodynamic polarization relating to corrosion rate, the susceptibility of certain alloys to corrosion and corrosion mechanisms by electrochemical reactions. Reddy et al. [26] Studied the effect of FSP on microstructural evolution and corrosion resistance of cast A356 alloy, and potentiodynamic polarization testing was used. It has been found that the friction in the processed zone exhibit enhanced corrosion. FSPed surface exhibited improved resistance to pitting corrosion compared to as-cast alloy due to passive film formation, which remains more intact on the FS-processed specimen's surface than as-cast specimens. This is attributed to the uniform distribution of fine, rich-silicon eutectics throughout the α-Al matrix due to mixing and

Accepted Manuscript

intense plastic deformation during FSP [26]. Table 1 shows a summary of previous reports of FSP effect's on cast aluminum alloys' properties.

In the above view, the influence of the FSP on the microstructural assessment, wear, hardness, and corrosion behavior of the Al-Si cast alloys, has not been sufficiently studied. Further studies are needed to improve Al-Si cast alloys' mechanical properties by implementing FSP with optimum parameters. Thus, modifying the surface structure of A356 cast alloy via FSP and studying its microstructural, hardness, tribological, and corrosion properties are the aims of this study.

Table 1 The effect of FSP parameters on properties of some cast Al alloys.

Material	Processing parameters	Enhanced property	Ref.
A365	- 300-900 rpm - 51,102, and 203 mm/min	- Refined grains were obtained, 3–4 μm - Low tool rotation rates of 300–500 rpm resulted in creating basin-like processed zones, whereas, at high tool rotation rates of 700–900 rpm, an elliptical processed zone with a typical onion ring structure was formed.	[21]
A319	- 800-1600 rpm - 22.2, 40, 75 mm/min	-YS has been increased by 13%, UTS was enhanced by 20 % to 50 %, and increases the EL from 1.5 to 5 times	[22]
Al-17%Si	- 664 rpm - 26, 40, 60 mm/min	-UTS has been increased 1.26 to 1.35 time. -EL has been increased from < 2 % to about 9 %.	[23]
A319	-1000 rpm -102 mm/min	- UTS of A319 was increased by 100%. The EL was increased by 1400%	[24]
A356	-1000 rpm -102 mm/min	-UTS of A356 was increased by 40%. The EL. was increased by 500 %.	[24]
Al-12%Si	-1250 rpm -65 mm/min	-UTS was increased by 50%. The EL was increased by 600%. - The hardness was increased by 20 % -The WR by weight loss was decreased 50 %	[25]
A356	-2000 rpm -20 mm/min	- The hardness was increased by 60% -The WR was decreased by 1500% -The COF was decreased by 300% - Significant enhancement in corrosion resistance	[26]
A356	- 500-1250 rpm -50 mm/min	- Si particles size decreased to 3.5μm at 1250 rpm -The WR decreased by 200% at 1250 rpm	[27]

2. Materials and methods

In this work, the A356 cast alloy with chemical composition illustrated in Table 2 was investigated. The as-received casted ingots were cut into plates with dimensions of 300 × 50 × 10 mm.

Accepted Manuscript

Table 2 the nominal chemical composition of the investigated alloy (wt. %).

Element	Si	Mg	Ti	Fe	Ni	Cu	Others	Al
wt.%	7.7%	0.17%	0.089%	0.119	0.0015	0.0007%	<0.05%	rest

2.1. Friction stir processing

The FSP was performed via a vertical CNC milling machine in a single pass using two different tools, a threaded cylindrical pin profiled tool (TCP) and a square pin with a cylindrical corners pin tool (SCCP). Both tools have the same cylindrical shoulder with a diameter of 22 mm. Fig. 1 illustrates the schematic illustration of the processing tools and their main dimensions. In this work, the processing conditions were three traverse speeds (mm/min), 10, 20, and 40, and five tool rotational speeds (rpm), 355, 450, 560, 710, and 900. During the processing, the tools were tilted with an angle of 2°.

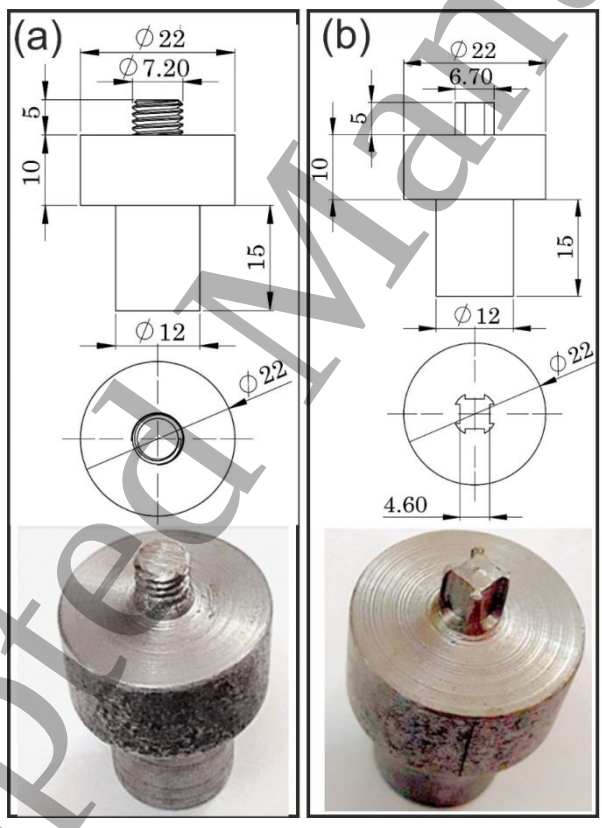

Fig. 1. The used FSP tools; (a) TCP and (b) SCCP

2.2. Microstructure analysis

The samples were taken perpendicular to the process direction (Fig. 2) and prepared for metallographic analysis according to the standard methods involving mechanical grinding,

Accepted Manuscript

polishing, and etching. The micro etching was performed using Keller's reagent for 5-120 s at room temperature. Microstructure characterization was performed on the samples using optical (OM) microscopy and scanning electron microscopy (SEM) joined with an energy dispersive X-ray (EDX) detector. The silicon particles were calculated using analyses of 3-5 micrographs using an AxioVision 4.5 software attached to the microscope (Carl Zeiss Oberkochen, Germany).

2.3. Hardness measurements

After FSP, samples for hardness measurements were cut along the transverse direction (Fig. 2). All samples were ground underwater on emery paper and then wet-polished to obtain a mirror finish. Vicker's microhardness tester with a load of 100 g and a shutter speed of 10 s was used to measure the hardness. Vickers microhardness ($HV_{0.1}$) profile was taken at the center of the SZ (the cross-section perpendicular to the process direction), and average values of seven readings at the center of the stir zone were applied for further analysis and investigation

2.4. Wear Testes

Dry sliding wear tests were carried out using a pin-on-ring machine (TNO equipment Delft, Netherlands) for the as-cast and FS processed samples. The wear specimens were cut perpendicular to the process direction (Fig. 2), having dimensions of 10×10×10 mm^3. Wear experiments were performed out for 20 minutes at a constant rotational speed of 100 rpm and a load of 50 N on the 316 stainless steel counterface cylinder (200 mm in diameter). Before each test, acetone was used to clean the cylinder to remove any surface pollutants. The rate of wear was calculated by weighting the samples after and before the wear tests via an electronic precision balance with ±0.1 mg accuracy[34] via the following equation:

$$wear\ rate\left(\frac{g}{cm^2}\right) = \frac{\Delta W}{A} \qquad 1$$

Where ΔW is the weight loss (g), and A is the area of the exposed surface to the friction (cm^2)

Accepted Manuscript

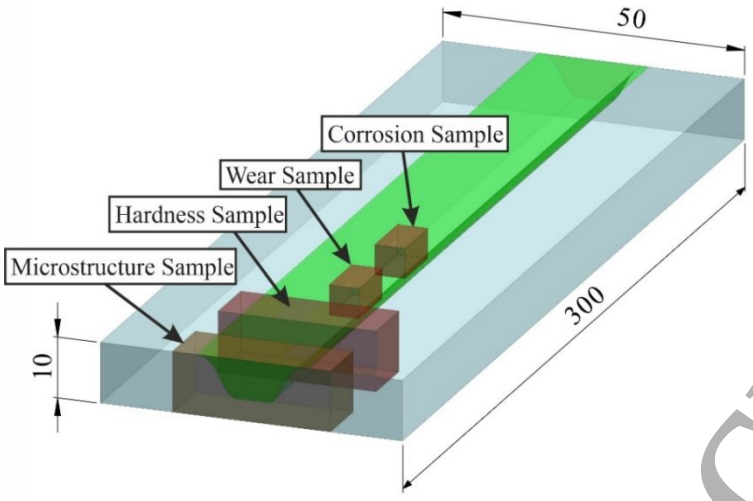

Fig. 2. The testing sample geometries were taken from the FSPed plate.

2.5. Corrosion tests

The corrosion behavior was studied using potentiodynamic polarization techniques in FSP zones (stir zone) and as-received alloy. The corrosion experiments were accomplished using workstation Autolab PGSTAT 302 N – High-Performance potentiostat/galvanostat instrument with NOVA 1.10 software. All experiments were performed using three conventional electrode cells; the reference Ag/AgCl, the platinum, and the working electrodes. At ambient temperature, the samples were immersed in a solution of NaCl, 3.5%. Polarization measurements were performed at potentials in the range of (-1.5 V to 1.5 V (SCE)) at a scan rate of 2 mVs^{-1}. For estimating the resistance polarization (Rp) and the corrosion rate by the cathodic and anodic polarization curves for the respective corrosion processes, the Tafel extrapolation was involved. FSPed samples for corrosion investigation were sectioned perpendicular to the direction of the process (Fig. 2). All exposed surfaces were wet-polished using emery paper of 1200 grit size, degreased in acetone, washed with distilled water, and dried by dryer before the electrochemical tests.

3. Results

3.1. Microstructural Characterization

Fig. 3 shows the macrostructure and microstructure of the different regions after FSP at a tool rotational speed of 355 rpm and a transverse speed of 10 mm/min vis the SCCP tool. The FSP changes the microstructure according to the distance from the used tool resulting in complex microstructures and heat dissipation zones across the section. The as-cast-based metal (BM) consists of primary Si particles, the α-Al phase (dendritic structure), and eutectic Al-Si needles.

Accepted Manuscript

The stirred zone (SZ) is the fully processed zone caused by the stirring action having a refined and homogenous structure. The Si particles are almost equiaxed in shape and uniform in size and distribution than that of the as-cast base metal. The heat from the plastic deformation regenerates the thermo-mechanically affected zone (TMAZ) and the heat-affected zone (HAZ). The microstructure of the nugget zone is very distinct from that of the A356 Al base alloy.

The (SZ) has much more uniformly distributed Si particles as compared to the BM. The FSP led to an essential breakup of acicular Si particles and α-Al dendrites, consequently producing a homogeneous microstructure of smaller broken Si particles in the α-Al matrix. It is noted that when the tool rotation speed was high, the transitional zone, which between the SZ and BM, was wider. When the tool rotation speed was low, the transitional zone was sharp. The main cause of the wider of the sharp zone is the generated heat during the process. High rotational speed results in high generated heat lead to a wider zone. The Advancing side, the right side in Fig. 3, is the location from where the solid material starts to transform into a semi-solid one and flows around the tool pin plunged into the material. This semi-solid material is retreated and cooled in the retreating side. Therefore, the advancing side has a more solid-state nature than the retreating side during FSP, which generates higher friction stress (unbalanced frictional force), which generates more heat and raises the peak temperature in the advancing side than the retreating side [21]. Besides, on the advancing side, being in the initial state of base metal undergoes the highest amount of plastic deformation in the entire shear zone. This plastic deformation also adds much heat there. Thus, the retreating side exhibits finer Si-particles and grains than those on the advancing side.

Fig. 4 shows the influence of FSP on the SZ microstructure of investigated alloy using both TCP (Fig. 4a-c) and SCCP (Fig. 4d-f) tools at 10mm/min and various rotational tool speeds. The grain size increased with increasing the rotational speed within the studied range for both tools. The effect of transverse speed, rotational speed, and type of tool on the size of Si particles is shown in Fig. 5. Si particles' average size was increased by decreasing the transverse speed or increasing the tool rotational speed for both tools. It was also found that increasing the transverse speed from 10 to 40 mm/min, at a constant tool rotational speed of 710 rpm and using The SCCP tool reduced the average size and aspect ratio of Si particulates from 2.07 to 1.6 μm and 2.72 to 2.09, respectively. At high traverse and rotational speeds, 40mm/min and 710 rpm, the SCCP tool exhibited a larger Si particle size than TCP. These results may attribute to the pulsating action of the SCCP that produces a high number of pulses. The pulsating action is due to the flat sides of the tool. There is no such pulsating action produced by the TCP. The

Accepted Manuscript

pulsating action generates heat slightly higher than the TCP tool resulting in a larger Si-particle size by using SCCP tool. At 10 mm/min, both tools' resulted Si particles' size has the same trend and characterization with the rotational speed. The result shows that the Si particles' mean size increases with increasing the tool rotational. In general, when the tool rotation speed was low, better particle refinement of the microstructure of the cast A356 alloy. Increasing the tool's rotation rate increases heat input through the FSP that influences Si particles' size. With increasing heat input, the Si particles' size should be increased [35, 36].

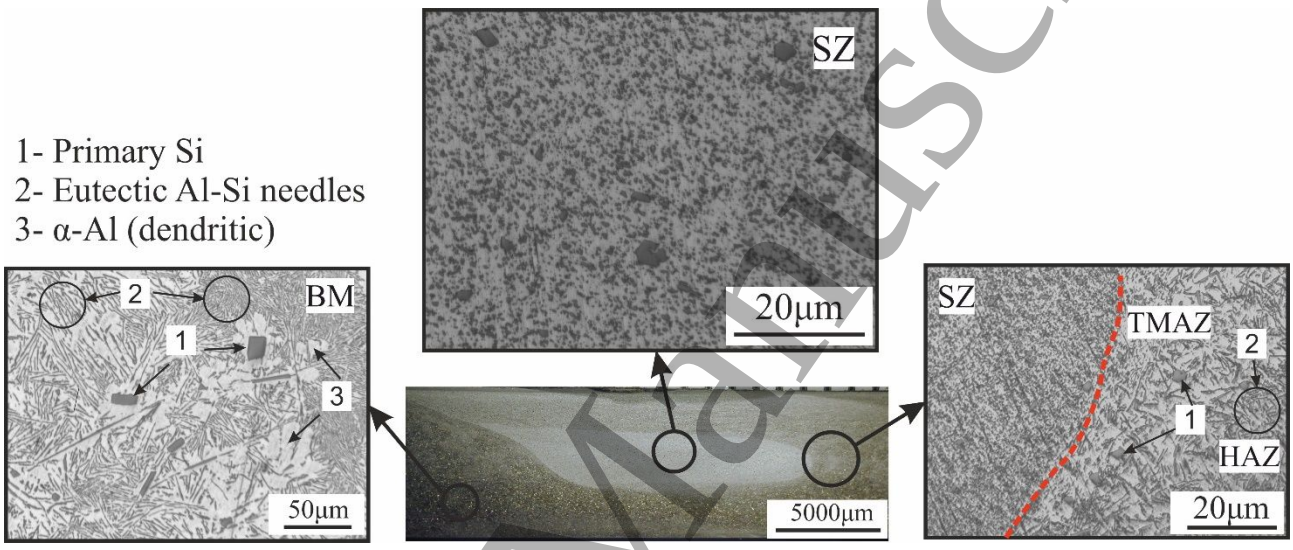

Fig. 3. Micrograph of FSPed sample at 10 mm/min and 355 rpm via SCCP tool showing the region of microstructural characterization; base metal BM, stirred zone SZ, thermomechanical affected zone TMAZ, and heat-affected zone HAZ (the advancing side is the right side).

Accepted Manuscript

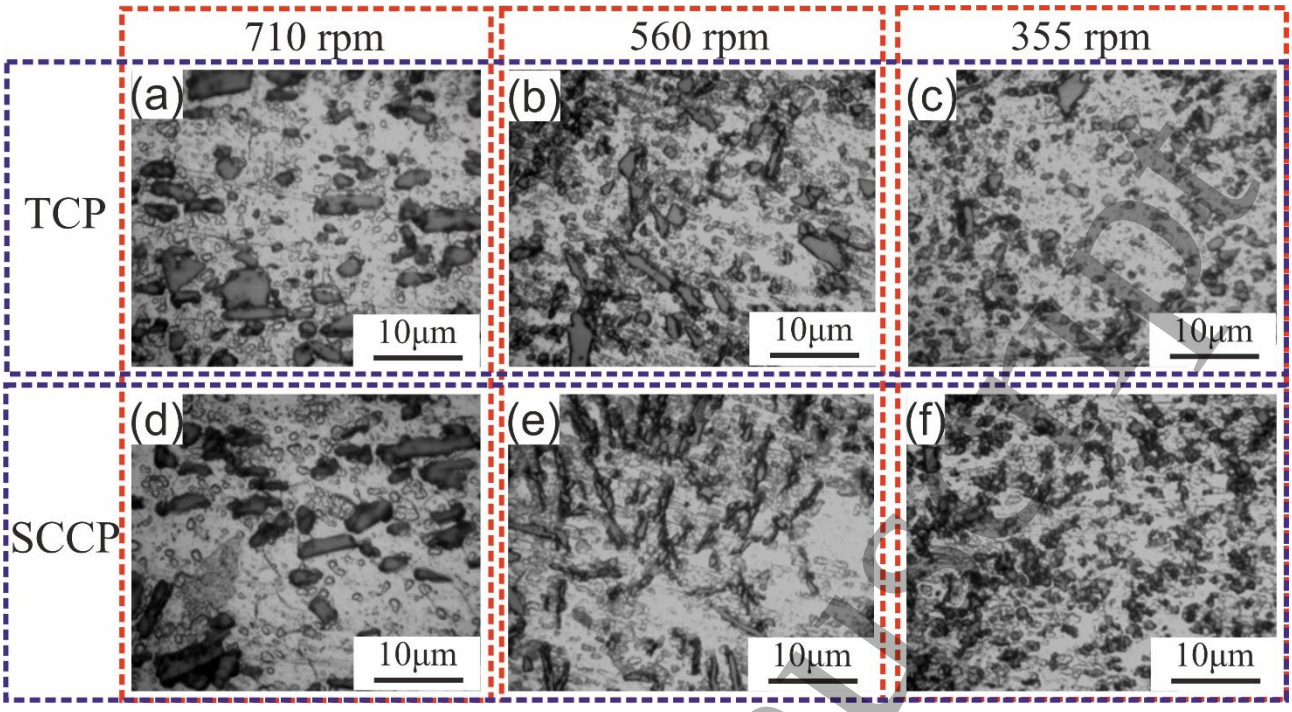

Fig. 4 Micrograph of the SZ of samples processed by (a-c) TCP and (d-f) SCCP at 10 mm/min and various tool rotational speeds; (a,d) 710 rpm, (b,e)560 rpm, (c,f) 355 rpm.

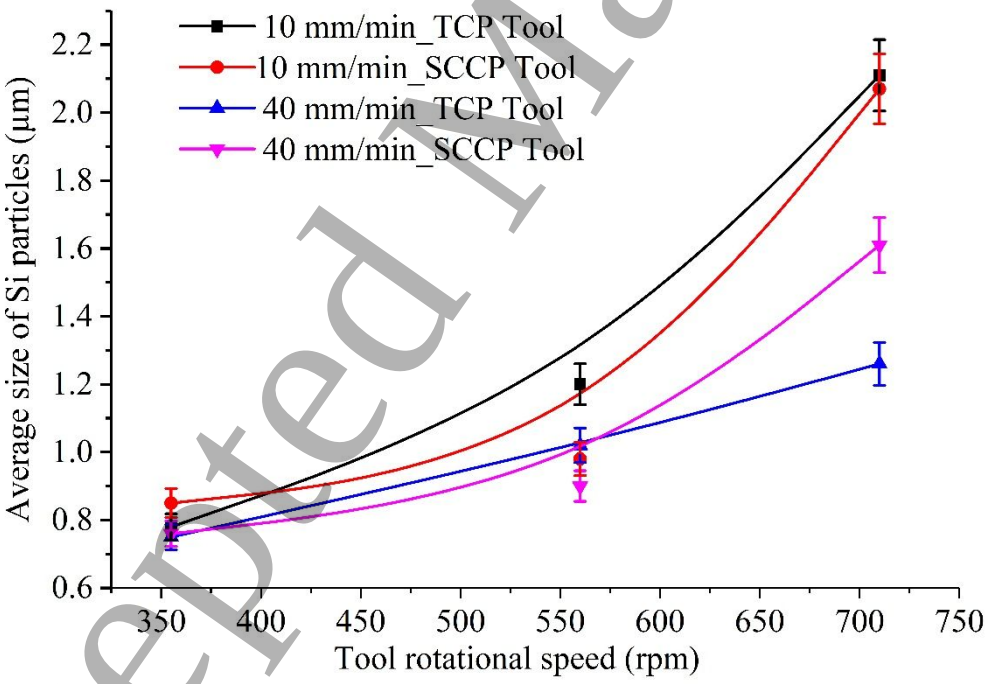

Fig. 5. Evolution of the average Si particles size with tool rotational speed at different transverse speeds using different tool geometry.

3.2. Microhardness measurements

Accepted Manuscript

The micro-hardness profiles along the centerline of the processed samples by TCP and SCCP tools at several FSP conditions are shown in Fig. 6a,b. The hardness variance with the tool rotational speed at multiple transverse speeds of both tools is presented in Fig. 6c,d. The as-cast A356 alloy exhibits hardness values 42±3 $HV_{0.1}$. The SZ hardness was remarkably higher than those of the BM for all conditions (Fig. 6).

For lower rotational speed, the SZ exhibited higher hardness values in the studied range of the traverse speed using both tools (Fig. 6,d). Increasing the rotational speed led to decreasing the hardness values though still higher than those of BM. On the other hand, the SZ hardness was observed to be increased with an increase in the transverse speed. The maximum hardness value of the SZ, 1.7 times of the BM, was obtained at 40 mm/min and 450 rpm processed via the TCP tool. Temperatures in the stirred zone rise as tool rotational speed increases. However, a large temperature increase causes grain growth, which causes the material to soften.

As a consequence, the hardness of the material can be decreased. Thus, the tool rotational speed must be moderate enough to avoid grain growth while at the same time providing the necessary heat to soften the material in order to ensure large plastic deformation, proper material flow, elimination of porosity, and grain refinement through recrystallization. Traverse feed rate also affects the strength/hardness of the processed material. At a specific tool rotational speed, with increasing traverse feed rate, the time of exposure of work material to frictional heat is decreased. This restricts grain growth. Therefore, it is important to increase the traverse feed rate sufficiently to limit grain growth, but not to such a high value that it does not allow the softening of the material and the consequent stirring by the tool pin. Also, the tool geometry plays a great role in heat generation. The best results were obtained in the present experiments at 450 rpm, 40 mm/min, and TCP tool.

Accepted Manuscript

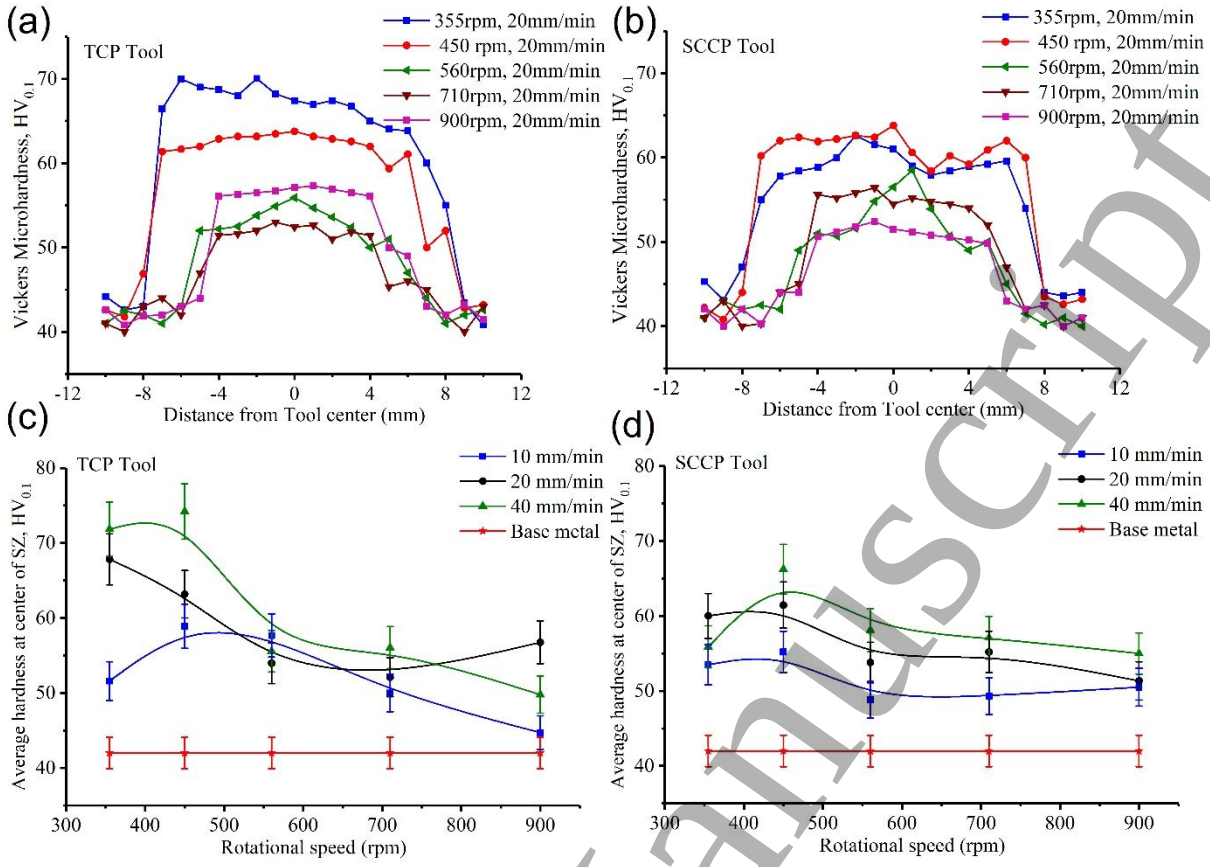

Fig. 6 (a,b) Vickers microhardness ($HV_{0.1}$) profiles of the SZ and (c,d) Average values of Vickers microhardness ($HV_{0.1}$) in SZ vs. the tool rotational speeds (rpm) by (a,c) TCP and (b,d) SCCP tools

3.3. Wear Behavior

The as-cast A356 alloy exhibited lower wear resistance than the FS-processed samples, and their WR was 2.41±0.25 g/cm^2. Fig. 7 presented the WR variations with the rotational speeds at multiple transverse speeds of the FSPed zones via TCP (Fig. 7a) and SCCP (Fig. 7b) tools. The samples processed at high rotational rates displayed lower wear resistance than those processed at lower rotation rates. The wear resistance of FSPed samples, on the other hand, has increased with an increase in transverse speed. The obtained WR at 900 rpm increased than 355 rpm by ten times using TCP tool (Fig. 7a) and 6 times using SCCP tool (Fig. 7b) at the same traverse speed 10 mm/min. At a rotational speed greater than 600 rpm, a substantial increase in WR was obtained.

Accepted Manuscript

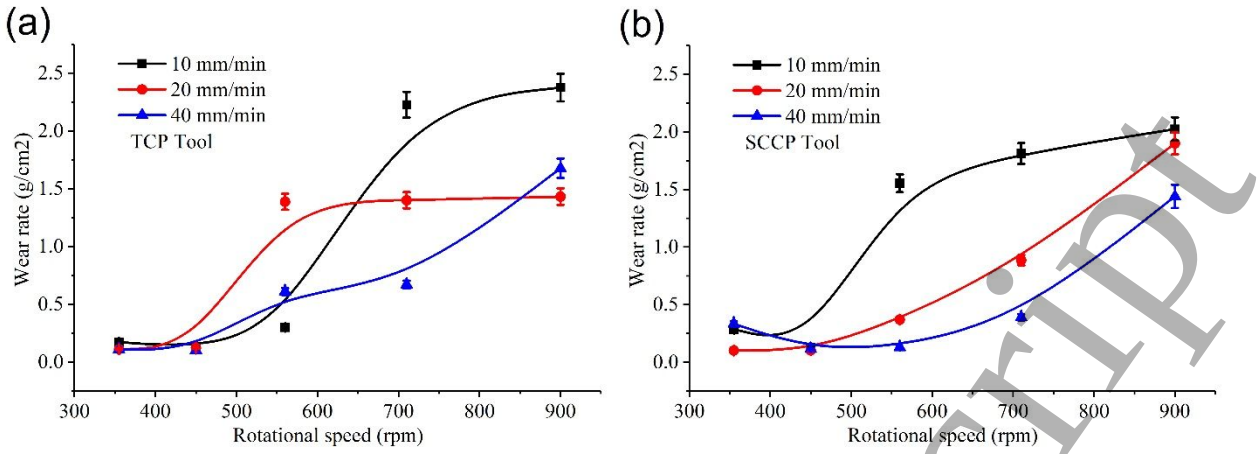

Fig. 7: Wear rate at the SZ with tool rotational speed (rpm) of samples prepared by (a) TCP and (b) SCCP tools

Fig. 8 and 9 show SEM micrographs of the worn surface for FSPed zones using the SCCP tool and at 450, 900 rpm, and 10, 40mm/min. The worn surfaces of FSPed zones at high tool traverse feed rates or low tool rotational speed exhibited smaller crack sizes and grooves (less damaged and smoother surfaces) (Fig. 8) than those of lower tool traverse feed rates or higher tool rotational speed (Fig. 9). The FS-processed samples at 10 mm/min and 900 rpm exhibited delamination and deep grooves on the worn surfaces with plastic deformation at the groove edge (Fig. 9a). The delamination and deep grooves on the worn surfaces were heavy in the case of 10 mm/min compared to those at 40 mm/min for the same rotational rate (Fig. 9b). The comparison of worn surfaces in Fig. 9 and Fig. 9 revealed the enhancement in this alloy's wear resistance at lower tool rotational/higher transverse speed. The main cause of lower WR at lower rotational speed is the homogenous distribution of fine Si particulates throughout the Al alloy and the absence of coarse dendrites might have decreased friction between the rotating disc and the pin. At high rotational speed and lower traverse speed, the generated heat was enough for grain growth resulted in higher friction and higher WR.

Accepted Manuscript

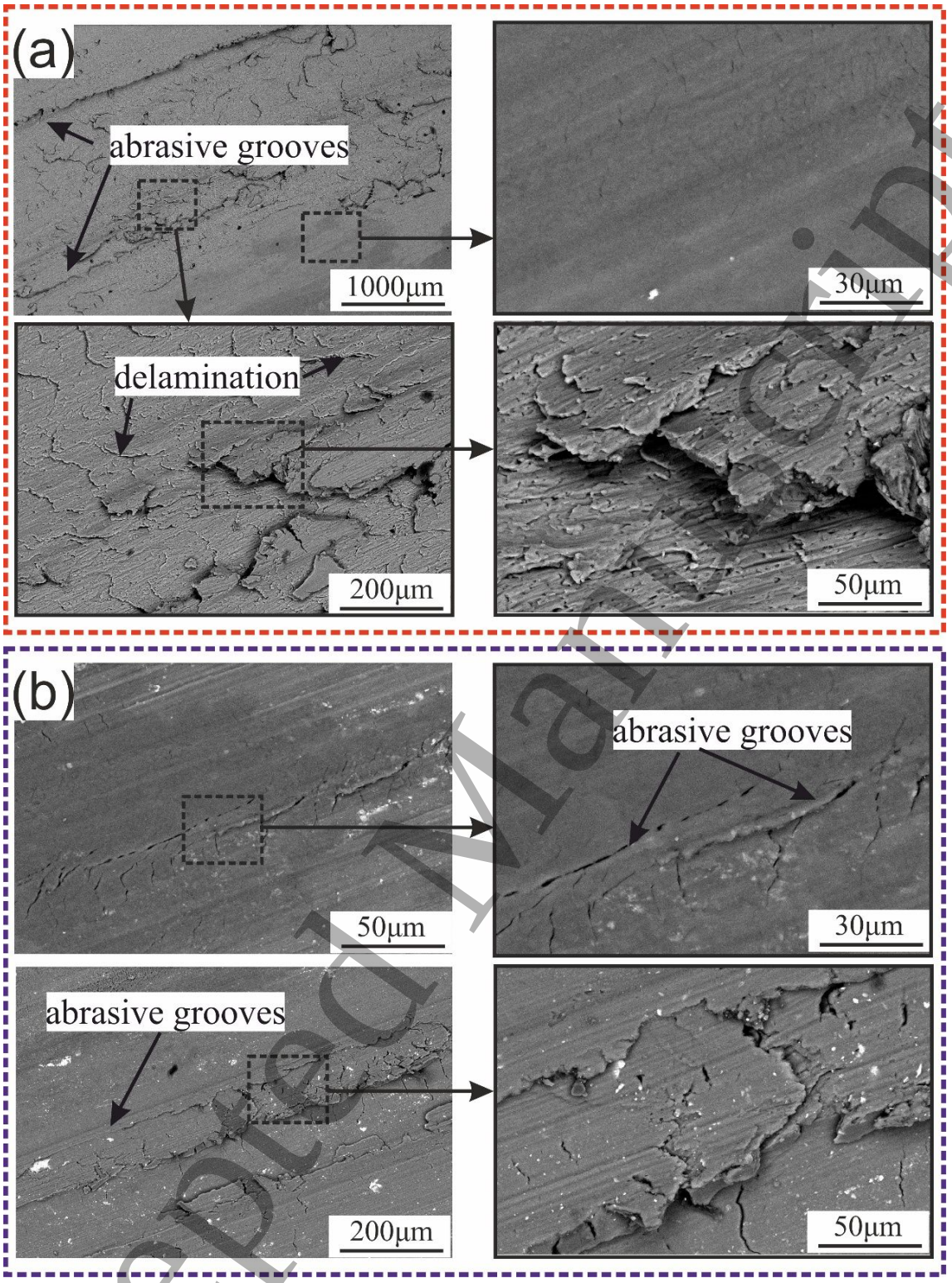

Fig. 8: SEM of the worn surface of FSPed samples at (a) 10 mm/min and (b) 40 mm/mm min and at 450 rpm prepared via SCCP pin

Accepted Manuscript

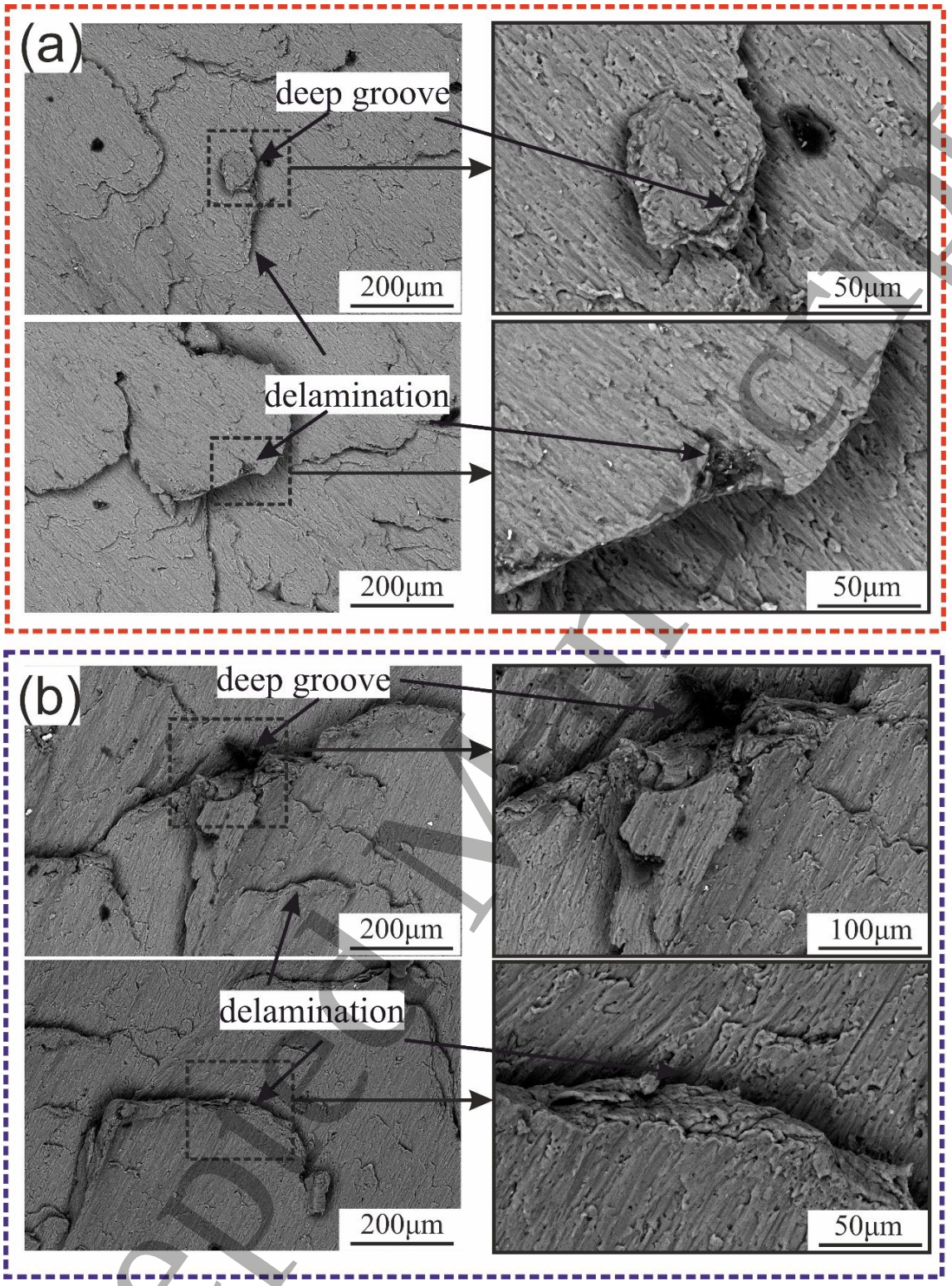

Fig. 9: SEM of the worn surface of FSPed samples at (a) 10 mm/min and (b) 40 mm/min and at 900 rpm prepared via SCCP tool.

Accepted Manuscript

3.4. **Corrosion Behavior**

Fig. 10 presents the BM and the FSP samples' potentiodynamic polarization plots at different rotational and traverse speeds using TCP (Fig. 10a-c) and SCCP (Fig. 10d-f) tools. The corrosion potential (E_{corr}) varies from one FSPed specimen to another depending on the microstructure, grain size, and Si particles' homogeneity. The values of E_{corr} are approximately in the domain of -0.69 to -1.19 versus SCE. The value for the base metal is about -0.92. So, in almost all instances, the base metal is more reactive than the FSPed specimens. This indicates the enhancement of corrosion resistance after FSP compared to as-cast samples. The enhancement in corrosion resistance may result from the grain refinement after the friction stir processing in which the Silicon-rich eutectics are distributed uniformly in the aluminum matrix.

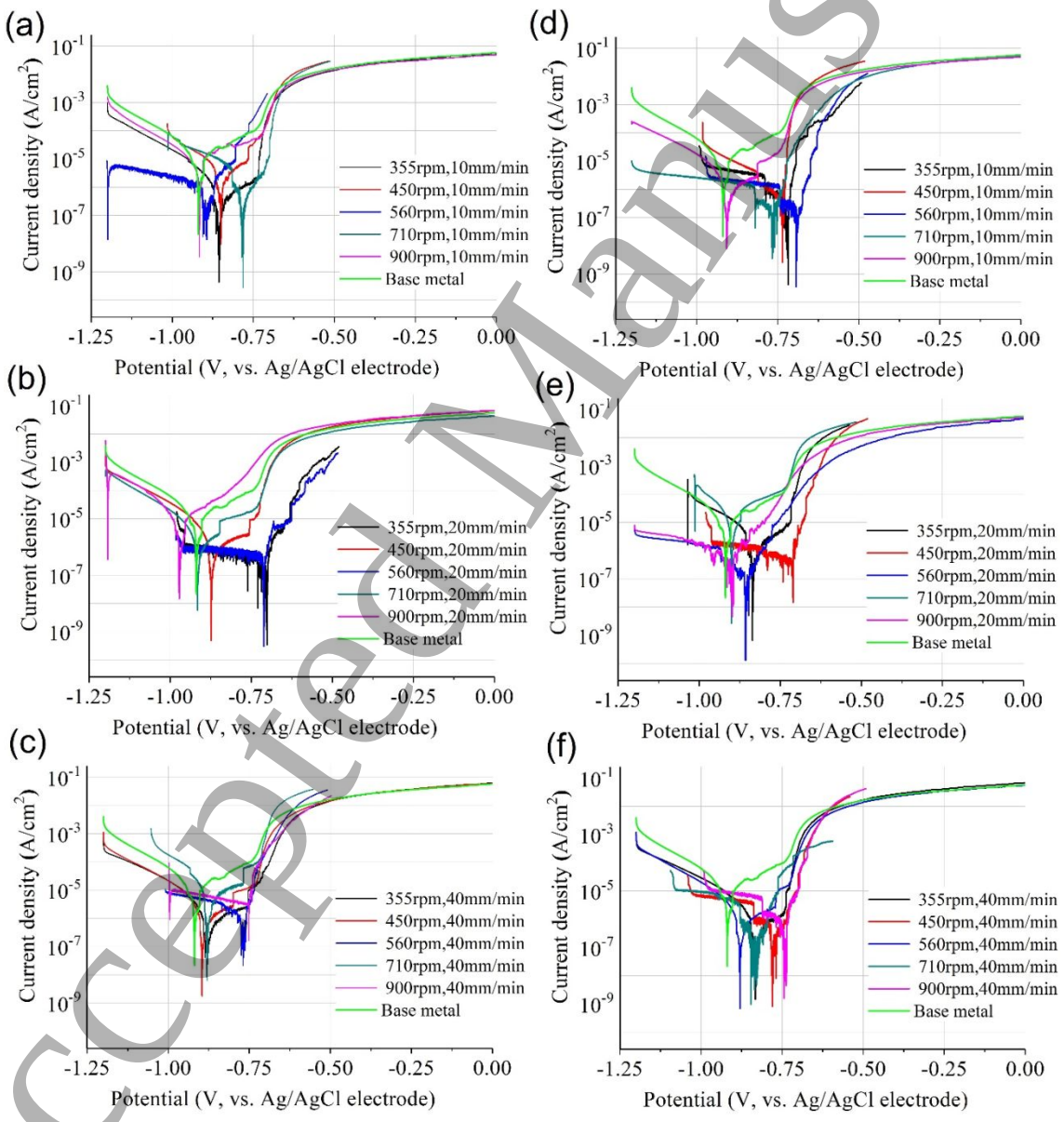

Fig. 10. Potentiodynamic polarization plots of the as-cast and SZ samples using (a-c) TCP and (d-f) SCCP tools

Accepted Manuscript

Fig. 11 shows the corrosion rates in the stirred zones processed at different rotational and traverse speeds using different process parameters of both TCP and SCCP tools. There is no significant difference in corrosion rate at lower rotational speed in the studied range of the traverse speed using both tools. Processing by the TCP tool, the corrosion rate suddenly increases at a rotational speed higher than 710 mm/min (Fig. 11a). The corrosion rate for the SCCP tool slightly increased at a rotational speed higher than 560 m/min (Fig. 11a). The maximum corrosion rate was obtained at 900 rpm and 10 mm/min. Generally, the TCP tool exhibited a higher corrosion rate than the SCCP tool at a higher rotational speed. Thus, the as-cast material exhibited higher corrosion rates, 0.02329 mm/year. It could be concluded that the corrosion resistance can be altered by altering the process parameters.

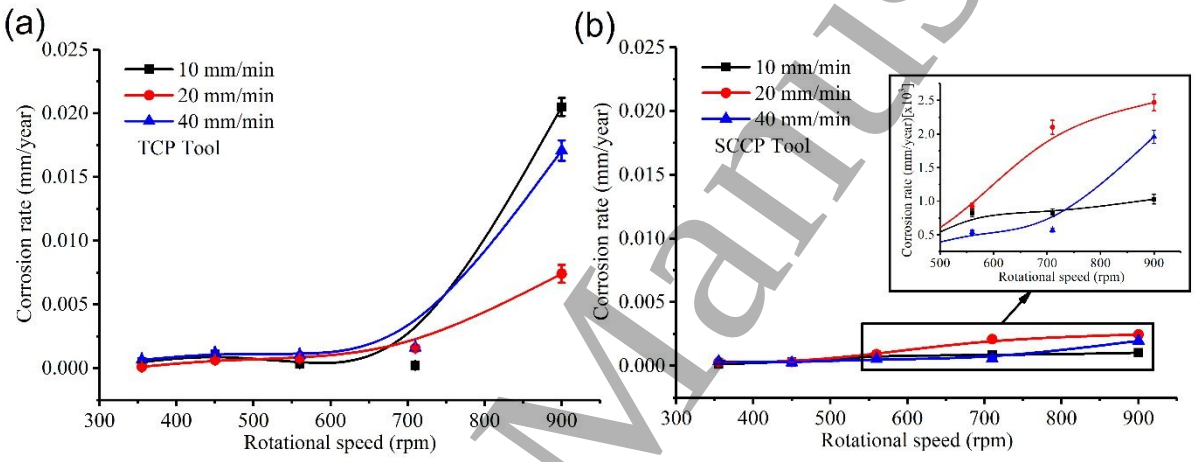

Fig. 11. Dependence of corrosion rate on rotational speeds of tools (a) TCP and (b) SCCP

The as-cast base alloy exhibited higher rates of corrosion and lower resistance to polarization than FSPed samples. The corrosion resistance improvement at lower rotational speed can be due to the decrease in the mean size/aspect ratio of the Si-particles and SZ's grain size. At lower rotational/higher traverse speed, the microstructure of the A356 was more refined than those at lower traverse speed / higher rotational. Increasing the rotation rate/decreasing traverse speed of the tool increases heat input through the FSP that influences the size/aspect ratio of Si-particles. Increasing the heat input, the size/aspect ratio of the Si-particles should be increased as mentioned by [35–37]. Thus, the corrosion resistance can be altered by altering the process parameters.

Fig. 12 shows the SEM images and EDX microanalysis of BM after electrochemical corrosion. After electrochemical corrosion, two different regions were marked by A (dark) and B (light). The EDX microanalysis of corroded products indicates that these regions exhibited different

Accepted Manuscript

chemical compositions. Region (A) have Si higher than Al contents than the region (B). The corrosion film formed is known to be SiO_2 and lower Al_2O_3 particulates. EDX for region "B revealed high concentrations of oxygen and aluminum (Al_2O_3 particulates) (Fig. 12). The corrosion product on the surface of the specimen is a porous surface due to highly oxide layers. Examining each specimen of electrochemical corrosion's SEM photos revealed that pitting and general corrosion is the primary corrosion mechanism.

Fig. 13 presented the SEM images after electrochemical corrosion of FSPed samples at 10 mm/min and lower tool rotational speed of 355 and 560rpm. It can be noted that at lower rotational tool speed, the material exhibits a lower corrosion rate. The specimen's surface at 355 rpm, 10 mm/min, and processed by TCP tool profile showed only local corrosion (small pits were ~ 23 to 12 µm) (Fig. 13a). Increasing the rotational speed to 560rpm, the size of the pits increased (Fig. 13b).

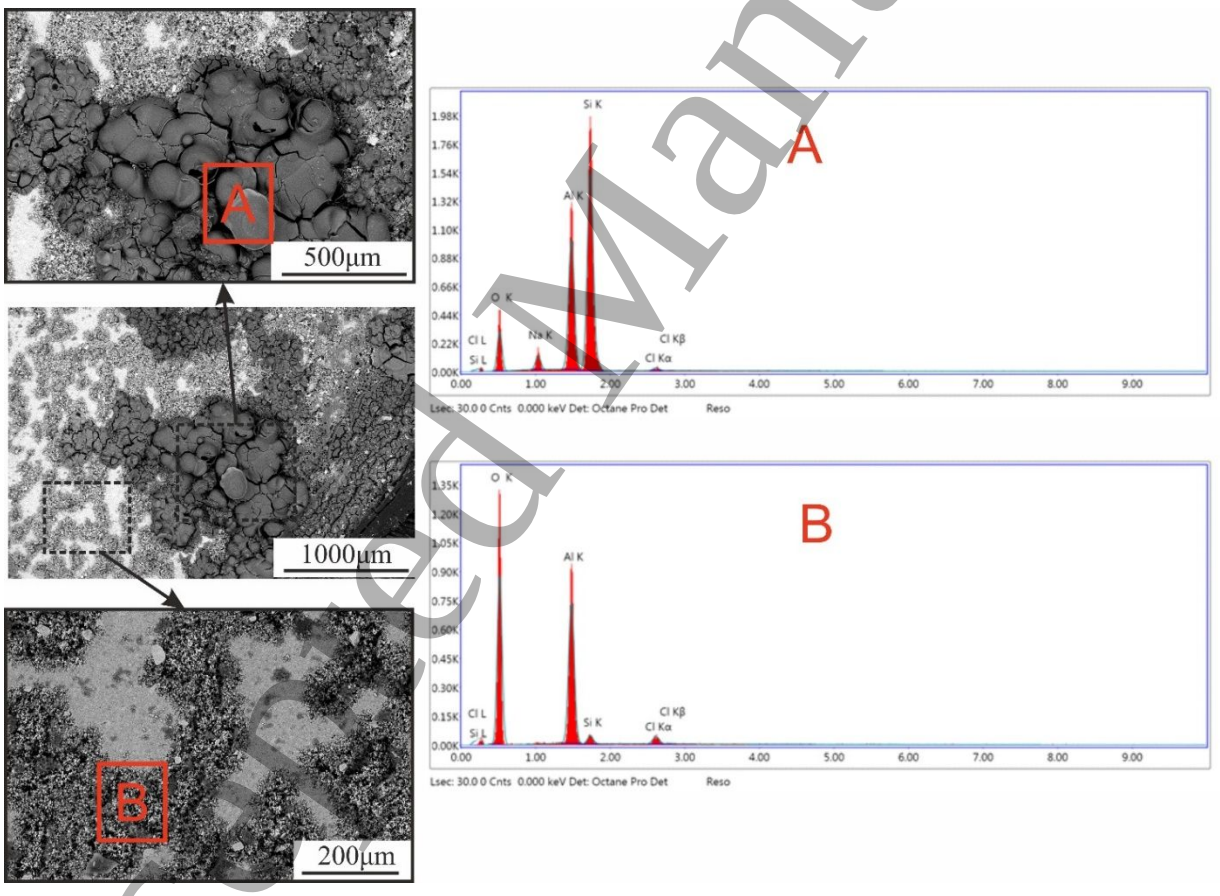

Fig. 12: SEM images of the corroded surfaces of as-cast (BM) and EDX spectra after polarization test in NaCl, 3.5%

Accepted Manuscript

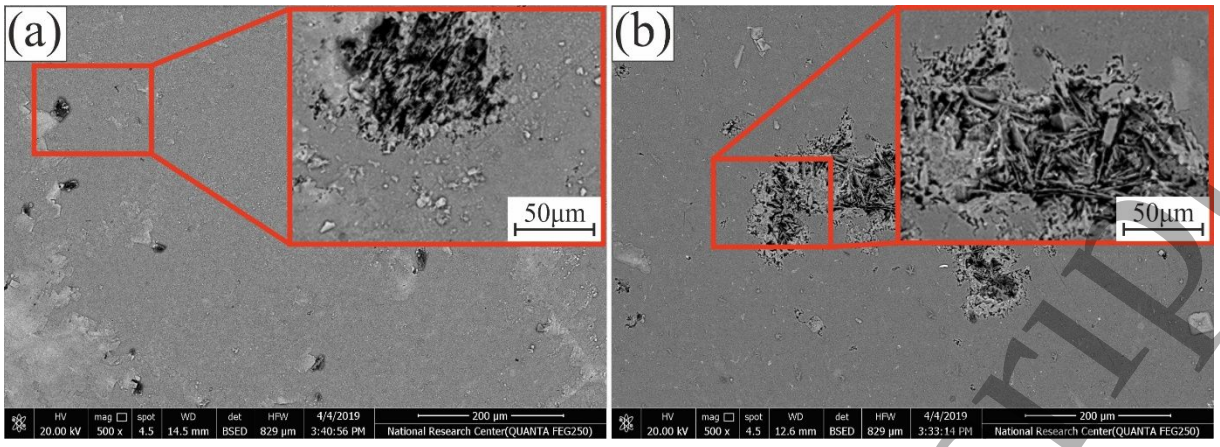

Fig. 13**.** The SEM images of the corroded surfaces at the stirred zones for FS Processed samples at (a) 10 mm\min and 355 rpm processed by SCCP and (b) 10 mm\min and 560 rpm processed by SCCP.

Fig. 14 shows the SEM images after electrochemical corrosion of FSPed samples at rotational tool speed of 900 rpm and transverse speed of 10 and 20 mm/min using TCP tool. Generally, these samples experienced the most severe corrosion attack noted in this study. Such results indicate that increasing the tool rotational speed decreases the corrosion resistance of the stirred zones. It is suggested that improvements in FSPed samples' pitting corrosion resistance compared to BM were due to the development of a passive film created by covering oxide layers on the FSPed samples' surface. Reducing the rotational speed of FSP resulted in a refined microstructure and increased distribution homogeneity of silicon-rich eutectics in α – matrix, confirmed by [26,35]. This could cause more excellent corrosion resistance for pitting.

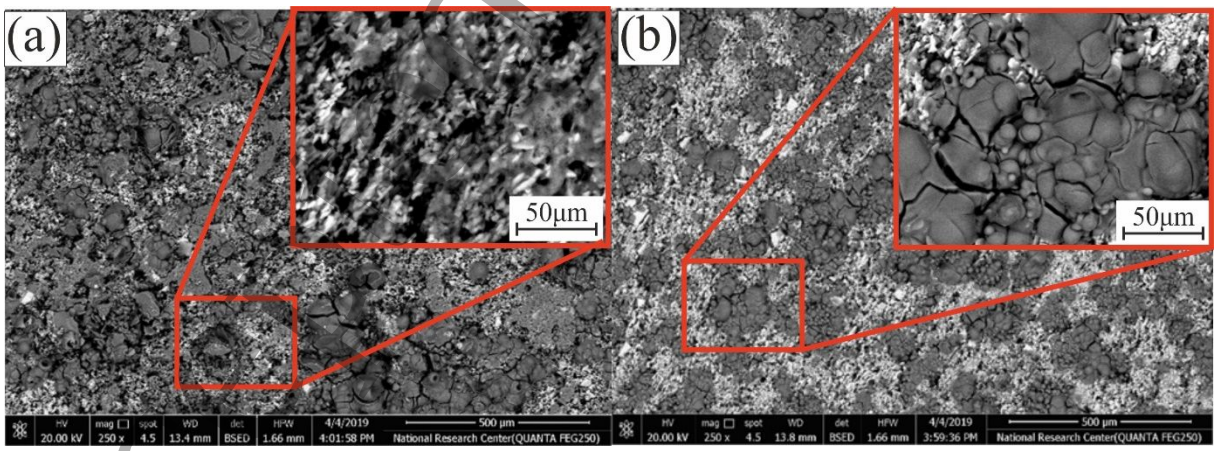

Fig. 14**.** The SEM images of the corroded surfaces at the stirred zones for FS Processed samples at (a) 10 mm\min and 900 rpm processed by TCP and (b) 20 mm\min and 900 rpm processed by TCP.

Accepted Manuscript

4. Discussion

The microstructure (grain size and distribution) is affected by the processing parameters of the FSP (tool geometry, rotational and traverse speed). After FSP, The SZ exhibited refined microstructure without a dendritic structure as compared to the BM. Reducing the processing speed/increasing tool rotational rate led to an increased mean size of the silicon particles within the stirred zone. The results are in agreement with [35–37]. Si particles' coursing at high rotational and lower traverse speed can be due to the dynamic recrystallization (DRX) during FS processing. The mean size of the silicon particles increases with increasing the rotation rate of the tool. In general, when the tool rotation rate was low, better particle refinement of the microstructure was achieved. Increasing the tool's rotation rate increased the heat input through the FSP, which influenced silicon particles' size. The tool geometry plays a vital role in material flow and affects the microstructure and Si particles size. SCCP tool produces pulsating stirring action in the flowing material due to the flat faces. There is no such pulsating action produced by the TCP. The pulsating action generates heat slightly higher than the TCP tool, resulting in larger Si-particle size using the SCCP tool. Such effect was noted in [10]

The as-cast BM exhibited scattering hardness around 43 MPa. The variance in the BM's hardness values can be due to the non-uniform distribution of the coarse acicular Si-particles within the Al-matrix. The SZ's hardness profiles displayed more uniform shapes, which were due to a homogeneous distribution of refined Si-particles in the Al-matrix and grain refining of the α-A1 grains and the elimination of casting defects such as pores and cavities [38]. The SZ has hardness values higher than both TMAZ and HAZ. The varying hardness with the rotational and traverse speed proved the hardness's dependence on the process parameters. The rotational speed is directly connected with the hardness. There was no direct relationship between the pin profile tools and the hardness. SZ's hardness increased by reducing the tool rotational speed or increasing the traverse feed rate. Reducing the tool's rotational rate reduced heat input, reducing dynamic recrystallization potential, which influences the Si particles size in agreement with [37].

The excellent wear resistance after the FSP is attributed to the uniform distribution of fine Si-rich eutectics over the α-aluminum matrix because of mixing and extreme plastic deformation through FSP. This result is in agreement with [25,26]. The decrease in the wear resistance of the FSPed zones with increasing the tool's rotation rates is due to a decrease in the SZs hardness with an increase in the tool rotation rates, as confirmed by [9,39]. The WR is influenced by the morphology, size, and distribution of silicon particles in the FSP of the A356 specimens. Large and irregularly shaped silicon particles concentrate the stress at the

Accepted Manuscript

boundaries of the silicon/matrix interfaces, which are generally considered to offer a convenient path for nucleation and spread of cracks. This leads to the shattering of large silicon particles into much smaller particles that can be separated from the surface and more inclined to fragment by the delamination wear process and behaves as another body abrasives increase WR [22,27].

The improvement in corrosion resistance may be attributed to using mechanical work during the FSP and the refinement microstructure in which the Si-rich eutectics are distributed uniformly in the aluminum matrix. This result is consistent with the results noted by many workers, such as [1–3]**.** Reducing the tool rotational speed increases the corrosion resistance of the stirred zones. The pitting corrosion resistance enhancements were due to passive film formation by covering oxide layers on the FS processed surface. This film stays more intact on the surface of the FSPed specimen than the as-cast specimen. FSP at a lower rotational speed resulted in a refined microstructure and increased homogeneity distribution of Si-rich eutectics in alpha–matrix [26]. This could increase resistance to pitting corrosion. The corrosion resistance of the BM and the stirred zones at high tool rotational speeds was reduced because of the early institution of the local galvanic action cells of corrosion between α-Al and coarse acicular Si particulates. The intensity of corrosion with galvanic coupling is determined by galvanic action with an area ratio of the cathode to anode due to large Si particles that accelerated the corrosion rate [40]. This finding is also consistent with the Hall – Petch type relationship, which is the pitting potential and the corrosion rate is inversely proportional to the grain and silicon particle sizes [41].

4. Conclusion

The influence of the FSP parameters (tool geometry, rotational and traverse speed) on the microstructure, hardness, wear, and corrosion behaviors of A356 aluinium alloy was studied. The main conclusions and findings can be summarised as follows;

1- Microstructure observation revealed that the FSP fragmented the needle-shaped eutectic and the primary silicon particles to a homogeneous microstructure having smaller broken silicon particles in the α-aluminum matrix. The mean size of silicon particles increases with increases rotational tool speed and decreases the traverse tool speed. The observed variation in particle size was more pronounced with increasing the rotational speed than the transverse speed and the pin profile tool geometry.
2- FSP significantly increased the SZ's hardness values than those of the BM, attributed to a homogeneous distribution of fine silicon particles in the aluminum matrix. Lower

Accepted Manuscript

rotational and higher traverse speed using the TCP tool are the optimum conditions for high hardness at the SZ after FSP.

3- An enhancement in wear resistance was obtained after performing the FSP on the investigated alloy. The improvement in wear resistance is owing to the homogeneous and refining microstructure of silicon particles and increased hardness.

4- The potentiodynamic polarization results showed higher rates of corrosion and lower resistance of the BM than FSPed samples. The primary corrosion mechanisms of the SZ and BM are pitting and general corrosion. The rotational speed has a clear relationship with the corrosion rate; as the rotational speed increased, the corrosion rate increased for stirred zones of FSPed specimens due to the increasing Si particle sizes.

References

[1] Clegg A J and Das A A 1977 Wear of a hypereutectic aluminium-silicon alloy *Wear* **43** 367–73

[2] Ward P J, Atkinson H V, Anderson P R G, Elias L G, Garcia B, Kahlen L and Rodriguez-ibabe J-M 1996 Semi-solid processing of novel MMCs based on hypereutectic aluminium-silicon alloys *Acta Mater.* **44** 1717–27

[3] Rao A G, Ravi K R, Ramakrishnarao B, Deshmukh V P, Sharma A, Prabhu N and Kashyap B P 2013 Recrystallization Phenomena During Friction Stir Processing of Hypereutectic Aluminum-Silicon Alloy *Metall. Mater. Trans. A* **44** 1519–29

[4] AbuShanab W S and Moustafa E B 2020 Effects of friction stir processing parameters on the wear resistance and mechanical properties of fabricated metal matrix nanocomposites (MMNCs) surface *J. Mater. Res. Technol.* **9** 7460–71

[5] Moustafa E, Mohammed S, Sayed A-W C and El-Kady E-S Review Multi Pass Friction Stir Processing *Am. Sci. Res. J. Eng.* 98–108

[6] Moustafa E B and Mosleh A O 2020 Effect of (Ti–B) modifier elements and FSP on 5052 aluminum alloy *J. Alloys Compd.* **823**

[7] Moustafa E 2017 Effect of multi-pass friction stir processing on mechanical properties for AA2024/Al2O3 nanocomposites *Materials (Basel).* **10**

[8] Moustafa E B, Melaibari A and Basha M 2020 Wear and microhardness behaviors of AA7075/SiC-BN hybrid nanocomposite surfaces fabricated by friction stir processing

Accepted Manuscript

Ceram. Int. **46** 16938–43

[9] Mahmoud T S and Mohamed S S 2012 Improvement of microstructural, mechanical and tribological characteristics of A413 cast Al alloys using friction stir processing *Mater. Sci. Eng. A* **558** 502–9

[10] Mosleh A O, Mahmoud F H, Mahmoud T S and Khalifa T A 2016 Microstructure and static immersion corrosion behavior of AA7020-O Al plates joined by friction stir welding *Proc. Inst. Mech. Eng. Part L J. Mater. Des. Appl.* **230**

[11] Campbell J 2015 *Complete Casting Handbook: Metal Casting Processes, Metallurgy, Techniques and Design* ed J B T-C C H (Second E Campbell (Boston: Butterworth-Heinemann)

[12] Campbell J 2006 Entrainment defects *Mater. Sci. Technol.* **22** 127–45

[13] Tiryakioğlu M, Campbell J and Staley J T 2003 The influence of structural integrity on the tensile deformation of cast Al–7wt.%Si–0.6wt.%Mg alloys *Scr. Mater.* **49** 873–8

[14] Mahmoud T S 2013 Surface modification of A390 hypereutectic Al–Si cast alloys using friction stir processing *Surf. Coatings Technol.* **228** 209–20

[15] Liu F C, Hovanski Y, Miles M P, Sorensen C D and Nelson T W 2018 A review of friction stir welding of steels: Tool, material flow, microstructure, and properties *J. Mater. Sci. Technol.* **34** 39–57

[16] Moustafa E B and Mosleh A O 2020 Effect of (Ti–B) modifier elements and FSP on 5052 aluminum alloy *J. Alloys Compd.* **823** 153745

[17] Rhodes C G, Mahoney M W, Bingel W H and Calabrese M 2003 Fine-grain evolution in friction-stir processed 7050 aluminum *Scr. Mater.* **48** 1451–5

[18] Kwon Y J, Shigematsu I and Saito N 2003 Mechanical properties of fine-grained aluminum alloy produced by friction stir process *Scr. Mater.* **49** 785–9

[19] Ahmed M, Aziz E-S, Elmahalawi I and Al-Aiat M M 2014 Effect of Friction Stir processing on the microstructure and mechanical properties of Aluminum Alloy 7020 *12th International Conference on Mining,Petrolem and Metallurgical Engineering (MPM12)*

[20] Itharaju R R 2004 *friction stir processing of aluminum alloys* (University of Kentucky)

[21] Ma Z Y, Sharma S R and Mishra R S 2006 Effect of friction stir processing on the microstructure of cast A356 aluminum *Mater. Sci. Eng. A* **433** 269–78

[22] Karthikeyan L, Senthilkumar V S and Padmanabhan K A 2010 On the role of process variables in the friction stir processing of cast aluminum A319 alloy 710 *Mater. Des.* 31 761–71

Accepted Manuscript

[23] Saini N, Dwivedi D K, Jain P K and Singh H 2015 Surface Modification of Cast Al-17%Si Alloys Using Friction Stir Processing *Procedia Eng.* **100** 1522–31

[24] Santella M L, Engstrom T, Storjohann D and Pan T-Y 2005 Effects of friction stir processing on mechanical properties of the cast aluminum alloys A319 and A356 *Scr. Mater.* **53** 201–6

[25] Aktarer S M, Sekban D M, Yanar H and Purcek G 2017 Effect of friction stir processing on tribological properties of Al-Si alloys *IOP Conf. Ser. Mater. Sci. Eng.* **174**

[26] Reddy G M and Rao K S 2010 Enhancement of wear and corrosion resistance of cast A356 aluminium alloy using friction stir processing *Trans. Indian Inst. Met.* **63** 793–8

[27] Alidokht S A, Abdollah-Zadeh A, Soleymani S, Saeid T and Assadi H 2012 Evaluation of microstructure and wear behavior of friction stir processed cast aluminum alloy *Mater. Charact.* **63** 90–7

[28] Navaser M and Atapour M 2017 Effect of Friction Stir Processing on Pitting Corrosion and Intergranular Attack of 7075 Aluminum Alloy *J. Mater. Sci. Technol.* **33** 155–65

29] Surekha K, Murty B S and Rao K P 2008 Microstructural characterization and corrosion behavior of multipass friction stir processed AA2219 aluminium alloy *Surf. Coatings Technol.* **202** 4057–68

[30] Surekha K, Murty B S and Prasad Rao K 2009 Effect of processing parameters on the corrosion behaviour of friction stir processed AA 2219 aluminum alloy *Solid State Sci.* **11** 907–17

[31] Patil H and Soman S 2014 Corrosion Behaviour of Friction Stir Welded Aluminium Alloys AA6082-T6 *Am. J. Mater. Eng. Technol.* **2** 29–33

[32] Chen Z, Li S and Hihara L 2015 Microstructure, mechanical properties and corrosion of friction stir welded 6061 Aluminum Alloy *arXiv Prepr. arXiv1511.05507*

[33] Abdul Raheem K and Abid Ali Zuheir T 2012 study the effect of silicon addition on the corrosion behavior and dry sliding wear of cu al ni shape memory alloy *Iraqi J. Mech. Mater. Eng.* **12** 964–77

[34] Węglowski M S 2014 Microstructural Characterisation of Friction Stir Processed Cast AlSi9Mg Aluminium Alloy *Arch. FOUNDRY Eng.* **14** 75–8

[35] Kim Y G, Fujii H, Tsumura T, Komazaki T and Nakata K 2006 Effect of welding parameters on microstructure in the stir zone of FSW joints of aluminum die casting alloy *Mater. Lett.* **60** 3830–7

Accepted Manuscript

[36] Mahmoud T S, Gaafer A M and Khalifa T A 2008 Effect of tool rotational and welding speeds on microstructural and mechanical characteristics of friction stir welded A319 cast Al alloy *Mater. Sci. Technol.* **24** 553–9

[37] Hassan A S, Mahmoud T S, Mahmoud F H and Khalifa T A 2010 Corrosion behaviour of dissimilar A319 and A356 cast aluminum alloys joined by Friction Stir Welding (FSW) *WCE 2010 - World Congr. Eng. 2010* **2** 1185–91

[38] Shiba A O, Mohamed S S and Mahmoud T S 2018 Influence of Friction STIR Processing on the Microstructural , Hardness and Tribological Characteristics of A356 Cast Aluminium Alloy microstructural Characteristics 24–31

[39] Kumar A, Sharma S K, Pal K and Mula S 2017 Effect of Process Parameters on Microstructural Evolution, Mechanical Properties and Corrosion Behavior of Friction Stir Processed Al 7075 Alloy *J. Mater. Eng. Perform.* **26** 1122–34

[40] Gebril M A, Omar M Z, Mohamed I F, Othman N K and Abdelgnei M A H 2018 Corrosion Improvement and Microstructure Evaluation of SEM-Solid A356 Alloy by Ecap Process *J. Phys. Conf. Ser.* **1082**

[41] Rao A G, Katkar V A, Gunasekaran G, Deshmukh V P, Prabhu N and Kashyap B P 2014 Effect of multipass friction stir processing on corrosion resistance of hypereutectic Al–30Si alloy *Corros. Sci.* **83** 198–208

Accepted Manuscript